Structural Engineering and Mechanics, *Vol. 75, No. 4 (2020) 425-434*
DOI: https://doi.org/10.12989/sem.2020.75.4.425

Simulation of nonstationary wind in one-spatial dimension with time-varying coherence by wavenumber-frequency spectrum and application to transmission line

Xiongjun Yang[a], Ying Lei[b], Lijun Liu* and Jinshan Huang[c]

Department of Civil Engineering, Xiamen University, Xiamen 361005, China

(Received March 15, 2020, Revised May 15, 2020, Accepted June 2, 2020)

Abstract. Practical non-synoptic fluctuating wind often exhibits nonstationary features and should be modeled as nonstationary random processes. Generally, the coherence function of the fluctuating wind field has time-varying characteristics. Some studies have shown that there is a big difference between the fluctuating wind field of the coherent function model with and without time variability. Therefore, it is of significance to simulate nonstationary fluctuating wind field with time-varying coherent function. However, current studies on the numerical simulation of nonstationary fluctuating wind field with time-varying coherence are very limited, and the proposed approaches are usually based on the traditional spectral representation method with low simulation efficiency. Especially, for the simulation of multi-variable wind field of large span structures such as transmission tower-line, not only the simulation is inefficient but also the matrix decomposition may have singularity problem. In this paper, it is proposed to conduct the numerical simulation of nonstationary fluctuating wind field in one-spatial dimension with time-varying coherence based on the wavenumber-frequency spectrum. The simulated multivariable nonstationary wind field with time-varying coherence is transformed into one-dimensional nonstationary random waves in the simulated spatial domain, and the simulation by wavenumber frequency spectrum is derived. So, the proposed simulation method can avoid the complicated Cholesky decomposition. Then, the proper orthogonal decomposition is employed to decompose the time-space dependent evolutionary power spectral density and the Fourier transform of time-varying coherent function, simultaneously, so that the two-dimensional Fast Fourier transform can be applied to further improve the simulation efficiency. Finally, the proposed method is applied to simulate the longitudinal nonstationary fluctuating wind velocity field along the transmission line to illustrate its performances.

Keywords: nonstationary process; fluctuating wind; time-varying coherence; evolutionary power spectrum; wavenumber-frequency spectrum; proper orthogonal decomposition; Fast Fourier transform; transmission tower-line

1. Introduction

Wind loads in practical engineering often exhibit the nonstationary characteristics, which need to be modeled as nonstationary random processes, especially in extreme wind environments such as tornadoes, typhoons and downburst, the nonstationary characteristics of wind loads are more prominent. With the continuous appearance of modern large-span structures, more and more attentions have been paid to nonstationary wind loads, and the accurate and efficient numerical simulation of nonstationary processes is the premise for the study of the aerodynamic characteristics of structures (Huang *et al.* 2015, Zentner *et al.* 2016, Lin *et al.* 2017, Tao and Wang 2019). Currently, the time series method and the spectral representation method (SRM) are two main families of simulation methods for nonstationary random processes (Huang *et al*. 2020). Especially, SRM is based on the evolutionary power spectral density (EPSD) with clear physical models describing the time and spectral energy of nonstationary processes. So, SRM has the advantages of high accuracy, clear theory and unconditional stability, and has been widely used in the simulation of nonstationary random processes (Priestley, 1965, Liang *et al.* 2007, Li *et al.* 2013, Liu *et al.* 2016, Lin *et al.* 2018, Wu *et al.* 2018, 2019).

However, since the evolutionary power spectrum is the function of both frequency and time, the Cholesky decomposition will be carried out at each frequency point and time point during the simulation of the non-stationary random process. So, the decomposition times will be greatly increased. The interpolation method has been used in the simulation of stationary wind field, Ding *et al*. (2018) introduced the Lagrange interpolation to simplify the computation of Cholesky decomposition of the cross-spectral density matrix. Tao *et al*. (2018) discussed the effects of different interpolation functions, the interpolated points distribution, and interpolation intervals on the accuracy and efficiency of the calculation results. To improve the computational efficiency of SRM for the simulation of non-stationary wind filed, Tao *et al.* (2018) proposed efficient reduced-Hermite bifold-interpolation schemes, in which only fixed number of Cholesky decomposition is needed in each simulation. Also, Bao *et al.* (2019) conducted Cholesky decomposition at some specific

*Corresponding author, Ph.D.
E-mail: liulj214@xmu.edu.cn
[a] M.Sc. Student
[b] Ph.D., Professor
[c] Ph.D. Student

Copyright © 2020 Techno-Press, Ltd.
http://www.techno-press.com/journals/sem&subpage=7
ISSN: 1225-4568 (Print), 1598-6217 (Online)

points in the time and frequency domain considering the smoothness and continuity of cubic spline interpolation.

When the number of simulating points of the wind field becomes quite large, such as the simulation of wind field on the transmission tower-line system, the dimension of the power spectrum density matrix is too large to conduct the Cholesky decomposition. To solve such problem, Benowitz and Deodatis (2015) proposed a novel stochastic wave-based model with the specific expression of the wavenumber-frequency joint power spectrum. The method circumvents the complex Cholesky decomposition. Peng *et al.* (2017) presented a simulation method for multi-point nonstationary random processes based on wavenumber-frequency spectrum, and shown that the proposed approach may enhance the simulation efficiency by thousands of times when the simulation number is quite large. Some researchers (Chen *et al.* 2018, Song *et al.* 2018, 2019) extended the evolutionary wavenumber-frequency joint power spectrum to the simulation of homogeneous or nonhomogeneous fluctuating wind field in two-spatial dimensions, and proposed uneven discretization strategies to reduce the number of discrete points and computational cost.

Zhao *et al.* (2017) and Peng *et al.* (2018) discovered the time-varying coherence function in the measured nonstationary wind field, and there was a big difference between the calculated results of structural response with and without time-varying coherence function. Recently, Huang *et al.* (2020) applied S-transform-based method to measured typhoon winds to obtain time-varying wind coherence. So, the simulation of the nonstationary wind field with time-varying coherence function is of engineering signification. However, currently limited methods for the simulation of wind field simulation with time-varying coherent function are based on the traditional spectral representation method (Zhao *et al.* 2017, Peng *et al.* 2018, Bao *et al.* 2019). Due to the need for Cholesky decomposition, the simulation efficiency still needs to be improved, especially for the simulation of multi-variable wind field on the large-span structures or the transmission tower-line.

On the other hand, due to the coupling of frequency and time in the evolutionary power spectra of nonstationary processes, it is impossible to use the Fast Fourier transform (FFT) in trigonometric series superposition. Li *et al.* (2017) employed Taylor series expansion to separate the frequency and time in the decomposition spectrum. Peng *et al.* (2017) proposed proper orthogonal decomposition (POD) to separate the frequency and time variables in the EPSD and speed up the calculation using 2D FFT. Zhao *et al.* (2017) studied the spectral representation method of nonstationary wind field with time-varying coherence function, and also adopted POD to separate the frequency and time variables in EPSD.

In this paper, an efficient method is proposed for the simulation of one-spatial dimension nonstationary fluctuating wind field with time-varying coherence function based on the hybrid wavenumber-frequency spectrum and POD, which can avoid the time-consuming Cholesky decomposition and reduce the computing time due to the use of 2D FFT after variable separation using POD. The remaining part of the paper is organized as: In Sect. 2, the details of the proposed efficient simulation method are presented, which contain the description of one-spatial dimension nonstationary fluctuating wind field with time-varying coherence by SRM in Sect.2.1, the derivation of wavenumber-frequency spectrum for one-spatial dimension nonstationary fluctuating wind field with time-varying coherence is descried in Sect.2.2, and the factorization by POD and simulation scheme via 2D-FFT are presented in sect. 2.3. In Sect. 3, the proposed method is applied to the simulation of multivariable nonstationary wind field on transmission tower-line to validate the performance and effectiveness of the proposed method. Finally, some conclusions are presented in the conclusion part.

2. The proposed method via hybrid wavenumber-frequency spectrum and FFT

In the proposed simulation method, the multivariate nonstationary one-spatial dimension wind field with time-varying coherence function is transformed into one-dimensional nonstationary random waves in the space domain. The transform relationship between power spectral density with time-varying coherence and wavenumber-frequency spectrum is derived, and finally, the simulation of nonstationary wind field via hybrid wavenumber-frequency spectrum and 2D FFT can be deduced.

2.1 One- spatial dimension nonstationary fluctuating wind field with time-varying coherence

At the height z (one-spatial dimension wind field), the nonstationary wind velocity time history of point i, $U_i(t)$ can be expressed as the sum of the time-varying mean wind velocity and the fluctuating constituent as:

$$U_i(t)=\overline{U}(t)+u_i(t) \tag{1}$$

in which $\overline{U}(t)$ is the time-varying mean wind velocity, $u_i(t)$ is the nonstationary fluctuating wind. For a n point multivariate nonstationary random fluctuating wind field $\boldsymbol{u}(t)=[u_1(t)\ \ u_2(t)\ \ \cdots\ \ u_n(t)]^T$, the EPSD of the wind field with time-varying coherence can be constructed as:

$$\boldsymbol{S}(\omega,t)=\begin{bmatrix} S_{11}(\omega,t) & S_{12}(\omega,t) & \cdots & S_{1n}(\omega,t) \\ S_{21}(\omega,t) & S_{22}(\omega,t) & \cdots & S_{2n}(\omega,t) \\ \cdot & \cdot & & \cdot \\ \cdot & \cdot & & \cdot \\ S_{n1}(\omega,t) & S_{n2}(\omega,t) & \cdots & S_{nn}(\omega,t) \end{bmatrix} \tag{2}$$

where ω is circular frequency, $S_{ii}(\omega,t)$ is the auto-spectral density at point i, $S_{ij}(\omega,t)$ is the cross-spectrum density between points i and j.

$$S_{ij}(\omega,t)=\sqrt{S_{ii}(\omega,t)S_{jj}(\omega,t)}\ \rho_{ij}(\omega,t) \tag{3}$$

in which $\rho_{ij}(\omega,t)$ is the time-varying coherence function of the point i and j. The time-varying characteristics of the coherence function have been observed under extreme wind conditions in recent years, so the extended Davenport coherence function $\rho_{ij}(\omega,t)$ is employed herein as: (Zhao *et* *al.* 2017, Bao *et al.* 2019):

$$\rho_{ij}(\omega,t)=\exp\left(-\frac{\lambda\omega|\varepsilon|}{\pi\left(\bar{U}_i(t)+\bar{U}_j(t)\right)}\right)=\exp\left(-\frac{\lambda\omega|\varepsilon|}{2\pi\left(\bar{U}(t)\right)}\right)=\rho(\varepsilon,\omega,t) \tag{4}$$

where λ is a decay factor, usually λ = 7 for horizontal decay, ε is distance between the two horizontal points. $\bar{U}_i(t)$and $\bar{U}_j(t)$ is time-varying mean wind velocity which both equal to $\bar{U}(t)$ because this paper focus on the simulation of nonstationary wind along 1-D transmission line, the vertical dimension is ignored as a simplicity. Therefore, the coherence function is independent of point location and the subscript of the coherence function can be removed in Eq. (4).

The correlation between the cross-correlation function $R_{ij}(t, t+\tau)$ of two points i, j and the power spectral density is as follows:

$$\begin{aligned} R_{ij}(t,t+\tau)&=\int_{-\infty}^{+\infty}\sqrt{S_{ii}(\omega,t)S_{jj}(\omega,t+\tau)\rho_{ij}(\omega,t)\rho_{ij}(\omega,t+\tau)}\ e^{i\omega\tau}d\omega \\ &=\int_{-\infty}^{+\infty}\sqrt{S(\omega,t,x)S(\omega,t+\tau,x+\varepsilon)\rho(\varepsilon,\omega,t)\rho(\varepsilon,\omega,t+\tau)}\ e^{i\omega\tau}d\omega \end{aligned} \tag{5}$$

in which t is the lag time in the cross-correlation function, x is the spatial coordinate of the simulation point i.

2.2 Wavenumber-frequency spectrum for one-spatial dimension nonstationary fluctuating wind field with time-varying coherence

For a one-dimensional nonstationary random wave in the space domain $f(x,t)$, let $A(\kappa, \omega, x, t)$ be the modulation function on wavenumber, frequency, space and time, $Z(\kappa, \omega)$ be the random processes with orthogonal increments, $f(x,t)$ can be expressed as: (Priestley 1965, Peng *et al.* 2017, Chen *et al.* 2018, Song *et al.* 2018, 2019)

$$f(x,t)=\int_{-\infty}^{+\infty}\int_{-\infty}^{+\infty}A(\kappa,\omega,x,t)e^{i(\omega\tau+\kappa\varepsilon)}dZ(\kappa,\omega) \tag{6}$$

The wavenumber-frequency spectrum $S^{(W-F)}(x, \kappa, \omega, t)$ of the nonstationary non-uniform random waves is:

$$S^{(W-F)}(x,\kappa,\omega,t)=\left|A(\kappa,\omega,x,t)\right|^2 S^{(W-F)}(\kappa,\omega) \tag{7}$$

where $S^{(W-F)}(\kappa, \omega)$ is the corresponding stationary and uniform wavenumber-frequency spectrum. The cross-correlation function of two points i and j with distance ε and time lag τ can be determined by (Deodatis and Shinozuka 1989, Peng *et al.* 2017)

$$\begin{aligned} &R_{ij}(t,t+\tau) \\ &=\int_{-\infty}^{+\infty}\int_{-\infty}^{+\infty}\sqrt{S^{(W-F)}(x_i,\kappa,\omega,t)S^{(W-F)}(x_j,\kappa,\omega,t+\tau)}\ e^{i(\omega\tau+\kappa\varepsilon)}d\kappa d\omega \end{aligned} \tag{8}$$

Let the Fourier transform of the coherence function $\rho(\varepsilon,\omega,t)$ in terms of the spatial distance ε between point i and j defined as:

$$\beta(t,\kappa,\omega)=\frac{1}{2\pi}\int_{-\infty}^{+\infty}\rho(\varepsilon,\omega,t)\ e^{-i\kappa\varepsilon}d\varepsilon \tag{9a}$$

$$\rho(\varepsilon,\omega,t)=\int_{-\infty}^{+\infty}\beta(t,\kappa,\omega)e^{i\kappa\varepsilon}\,d\kappa \tag{9b}$$

Eq. (5) can be rewritten as:

$$\begin{aligned} R_{ij}(t,t+\tau)&=\int_{-\infty}^{+\infty}\int_{-\infty}^{+\infty}\sqrt{S(\omega,t,x_i)S(\omega,t+\tau,x_j)\beta(t,\kappa,\omega)\beta(t+\tau,\kappa,\omega)}\ e^{i\kappa\varepsilon}d\kappa e^{i\omega\tau}d\omega \\ &=\int_{-\infty}^{+\infty}\int_{-\infty}^{+\infty}\sqrt{S(\omega,t,x_i)\beta(t,\kappa,\omega)S(\omega,t+\tau,x_j)\beta(t+\tau,\kappa,\omega)}\ e^{i(\omega\tau+\kappa\varepsilon)}d\kappa d\omega \end{aligned} \tag{10}$$

By comparing the cross-correlation function of random wave in Eq.(8) with that of random process in Eq.(10), the transformation of evolutionary power spectrum density (EPSD) with time-varying coherence to the wavenumber-frequency spectral density $S^{(W-F)}(x,\kappa,\omega,t)$ can be derived as:

$$S^{(W-F)}(x,\kappa,\omega,t)=S(\omega,t,x)\cdot\beta(t,\kappa,\omega) \tag{11}$$

With Eq. (4) and Eq. (9a), the Fourier transform of the time-varying coherent function can be obtained as:

$$\beta(t,\kappa,\omega)=\frac{1}{2\pi}\int_{-\infty}^{+\infty}\rho(\varepsilon,\omega,t)\ e^{-i\kappa\varepsilon}d\varepsilon=\frac{\lambda\omega}{2\pi^2\bar{U}(t)}\frac{1}{\left(\frac{\lambda\omega}{2\pi\bar{U}(t)}\right)^2+\kappa^2} \tag{12}$$

After obtaining the wavenumber-frequency spectrum of the random process, the spectrum representation method can be used for sample simulation (Deodatis and Shinozuka, 1989) by:

$$u(x,t) = 2\sum_{m=1}^{N_\kappa}\sum_{l=1}^{N_\omega}\sqrt{S^{(W-F)}(x,\kappa_m,\omega_l,t)\Delta\kappa\Delta\omega}\begin{bmatrix}cos(\kappa_m x+\omega_l t+\phi_{ml}^{(1)}) \\ + cos(\kappa_m x-\omega_l t+\phi_{ml}^{(2)})\end{bmatrix} \tag{13}$$

where N_κ and N_ω is discrete points in the wavenumber domains and frequency domains respectively, $\kappa_m = m\Delta\kappa$, $\omega_l = l\Delta\omega$, $\Delta\kappa = \frac{\kappa_{up}}{N_\kappa}$, $\Delta\omega = \frac{\omega_{up}}{N_\omega}$, κ_{up} and ω_{up} are the truncation ceiling in the wavenumber domains and frequency domains, respectively, $\phi_{ml}^{(1)}$ and$\phi_{ml}^{(2)}$ are the two uniformly distributed in $[0.2\pi]$ and independent random variables.

Therefore, the wavenumber-frequency spectrum can be obtained by multiplying of self-power spectral density and the Fourier transform of time-varying coherence function, and then the simulation sample can be obtained. The proposed method does not require Cholesky decomposition and is suitable for the simulation of multivariable nonstationary random processes, especially for the simulation of wind filed on long span bridges or power transmission lines. However, due to the coupling of spatial and temporal variables with frequency and wavenumber variables in the wavenumber-frequency spectrum, it is impossible to directly use 2D FFT for trigonometric series superposition in Eq. (13), which is computational inefficiency.

2.3 Factorization by POD and simulation scheme via 2D-FFT

In the traditional spectral representation methods, many methods have been developed to decoupling variables, such as wavelet decomposition (Zhao *et al.* 2017), Taylor series expansion (Li *et al.* 2017), and POD (Huang, 2014). In the researches of wind field simulation based on wavenumber- frequency spectrum, Peng *et.al* (2017) used POD to decouple variables, and the algorithm is efficient, but the coherence function was assumed time-invariant. As POD is able to find the optimal orthogonal basis of matrix, the original matrix can be approximately reconstructed by using only a few feature vectors (optimal orthogonal basis), which dramatically reduce the matrix dimension. Therefore, POD is employed for variable separation in this paper. However, because of the influence of the time-varying coherence function, not only the spectral density $S(\omega, t, x)$ but also the Fourier transform of time-varying coherence function $\beta(t, \kappa, \omega)$ need to be decoupled. Therefore, the POD decoupling method is extended to treat time-varying coherence function in this paper, so that 2D FFT can be employed to accelerate the trigonometric series superposition.

Simply, $\beta(t, \kappa, \omega)$ and $S(\omega, t, x)$ can be expressed as matrices with $N_t \times N_\kappa \cdot N_\omega$ and $N_\omega \times N_t \cdot n$ dimensions, respectively

$$\mathbf{P} = \begin{bmatrix} \sqrt{\beta(t_1,\kappa_1,\omega_1)} & \sqrt{\beta(t_1,\kappa_1,\omega_2)}\cdots\sqrt{\beta(t_1,\kappa_1,\omega_{N_\omega})} & \sqrt{\beta(t_1,\kappa_2,\omega_1)}\cdots\sqrt{\beta(t_1,\kappa_{N_\kappa},\omega_{N_\omega})} \\ \sqrt{\beta(t_2,\kappa_1,\omega_1)} & \sqrt{\beta(t_2,\kappa_1,\omega_2)}\cdots\sqrt{\beta(t_2,\kappa_1,\omega_{N_\omega})} & \sqrt{\beta(t_2,\kappa_2,\omega_1)}\cdots\sqrt{\beta(t_2,\kappa_{N_\kappa},\omega_{N_\omega})} \\ \cdot & \cdot & \cdot \\ \cdot & \cdot & \cdot \\ \sqrt{\beta(t_{N_t},\kappa_1,\omega_1)} & \sqrt{\beta(t_{N_t},\kappa_1,\omega_2)}\cdots\sqrt{\beta(t_{N_t},\kappa_1,\omega_{N_\omega})} & \sqrt{\beta(t_{N_t},\kappa_2,\omega_1)}\cdots\sqrt{\beta(t_{N_t},\kappa_{N_\kappa},\omega_{N_\omega})} \end{bmatrix} \tag{14}$$

$$\mathbf{Q} = \begin{bmatrix} \sqrt{S(\omega_1,t_1,x_1)} & \sqrt{S(\omega_1,t_2,x_1)}\cdots\sqrt{S(\omega_1,t_{N_t},x_1)} & \sqrt{S(\omega_1,t_1,x_2)}\cdots\sqrt{S(\omega_1,t_{N_t},x_n)} \\ \sqrt{S(\omega_2,t_1,x_1)} & \sqrt{S(\omega_2,t_2,x_1)}\cdots\sqrt{S(\omega_2,t_{N_t},x_1)} & \sqrt{S(\omega_2,t_1,x_2)}\cdots\sqrt{S(\omega_2,t_{N_t},x_n)} \\ \cdot & \cdot & \cdot \\ \cdot & \cdot & \cdot \\ \sqrt{S(\omega_{N_\omega},t_1,x_1)} & \sqrt{S(\omega_{N_\omega},t_2,x_1)}\cdots\sqrt{S(\omega_{N_\omega},t_{N_t},x_1)} & \sqrt{S(\omega_{N_\omega},t_1,x_2)}\cdots\sqrt{S(\omega_{N_\omega},t_{N_t},x_n)} \end{bmatrix} \tag{15}$$

where N_t is the time index number, n denotes the number of simulation points. Since the time-varying coherence is considered in this paper, **P** in Eq. (14) is taken as an example to be carried out by eigenvectors decomposition. **R** is the covariance matrix of **P**, which can be obtained by (Deodatis and Shinozuka,1989)

$$\mathbf{R} = \frac{1}{nN_t}\mathbf{P}\cdot\mathbf{P}^T \tag{16}$$

$$\mathbf{R}\boldsymbol{\phi}_p = \lambda_p\boldsymbol{\phi}_p \tag{17}$$

in which λ_p and ϕ_p are the p-th eigenvalues and eigenvectors of **R** in Eq. (17), respectively. The eigenvalues λ_p are arranged from large to small. The first few eigenvalues contain most information of the matrix, so reduced-order model is obtained, and **P** can be reconstructed as (Peng *et al.* 2017):

$$\mathbf{P} \approx \sum_{p=1}^{N_p}\boldsymbol{\phi}_p\left(\boldsymbol{\phi}_p^T\mathbf{P}\right) = \sum_{p=1}^{N_p}\boldsymbol{\phi}_p\boldsymbol{a}_p \tag{18}$$

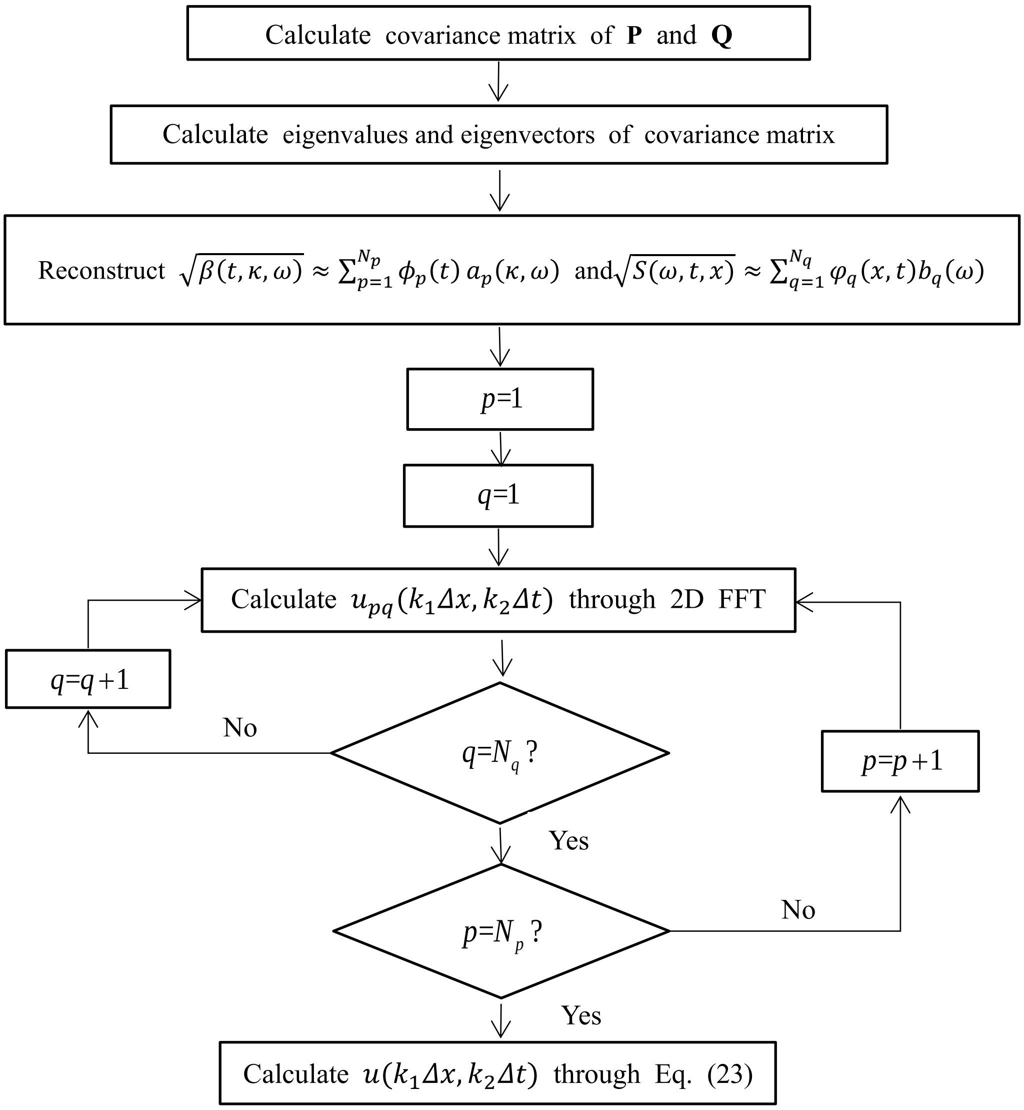

Fig. 1 Flow chart of the proposed algorithm

in which, N_p is module truncation order, $N_p \ll N_\omega$. Eq. (18) is rewritten as follow:

$$\sqrt{\beta(t,\kappa,\omega)} \approx \sum_{p=1}^{N_p} \phi_p(t) a_p(\kappa,\omega) \tag{19}$$

Similarly, **Q** in Eq. (15) could also be carried out by eigenvectors decomposition, and the calculated eigenvectors are used as the orthogonal basis, $\sqrt{S(\omega,t,x)}$ is reconstructed as

$$\sqrt{S(\omega,t,x)} \approx \sum_{q=1}^{N_q} \varphi_q(x,t) b_q(\omega) \tag{20}$$

Then, based on Eq. (11), Eq. (19) and Eq. (20), wavenumber-frequency spectrum can be reconstructed as

$$\sqrt{S^{(W-F)}(x,\kappa,\omega,t)} = \sum_{p=1}^{N_p} \phi_p(t) a_p(\kappa,\omega) \cdot \sum_{q=1}^{N_q} \varphi_q(x,t) b_q(\omega) \tag{21}$$

After POD for the separation of variables for both the time-space dependent evolutionary power spectral density and the Fourier transform of time-varying coherent function, 2D FFT can be adopted for efficient calculation of trigonometric series superposition.

By inserting Eq. (21) into Eq. (13), spectrum expression after variable separation can be derived as

$$\begin{aligned} u(x,t) &= 2\sum_{m=1}^{N_\kappa}\sum_{l=1}^{N_\omega}\left(\sum_{p=1}^{N_p} \phi_p(t) a_p(\kappa_m,\omega_l) \cdot \sum_{q=1}^{N_q} \varphi_q(x,t) b_q(\omega_l)\right)\sqrt{\Delta\kappa\Delta\omega} \cdot \left(cos\left(\kappa_m x + \omega_l t + \phi_{ml}^{(1)}\right) + cos\left(\kappa_m x - \omega_l t + \phi_{ml}^{(2)}\right)\right) \\ &= 2\sum_{p=1}^{N_p}\sum_{q=1}^{N_q} \phi_p(t)\varphi_q(x,t)\sum_{m=1}^{N_\kappa}\sum_{l=1}^{N_\omega} a_p(\kappa_m,\omega_l) b_q(\omega_l)\sqrt{\Delta\kappa\Delta\omega} \cdot \left(cos\left(\kappa_m x + \omega_l t + \phi_{ml}^{(1)}\right) + cos\left(\kappa_m x - \omega_l t + \phi_{ml}^{(2)}\right)\right) \end{aligned} \tag{22}$$

By adjusting the order of series superposition, Eq. (22) can be simplified as

$$u(x,t)=2\sum_{p=1}^{N_p}\sum_{q=1}^{N_q}\phi_p(t)\varphi_q(x,t)u_{pq}(x,t) \tag{23}$$

$$\begin{aligned} u_{pq}(x,t) = \sum_{m=1}^{N_\kappa}\sum_{l=1}^{N_\omega} & a_p(\kappa_m,\omega_l)b_q(\omega_l)\sqrt{\Delta\kappa\Delta\omega} \\ & \cdot\left(\cos\left(\kappa_m x+\omega_l t+\phi_{ml}^{(1)}\right)\right. \\ & \left.+\cos\left(\kappa_m x-\omega_l t+\phi_{ml}^{(2)}\right)\right) \end{aligned} \tag{24}$$

Eq. (24) can be expressed in discrete form:

$$u_{pq}(k_1\Delta x,k_2\Delta t)=\mathrm{Re}\left(E_{k_1k_2}^{pq}+\tilde{E}_{k_1k_2}^{pq}\right) \tag{25}$$

where Re $(\cdot)$ denotes real number, $k_1=1,2,\ldots M_1, k_2=1,2,\ldots M_2$. To avoid aliasing, $M_1\geq 2N_\kappa$ and $M_2\geq 2N_\omega$ are required. By the sampling theorem, $\Delta\kappa\Delta x=\frac{2\pi}{M_1}$, $\Delta\omega\Delta t=\frac{2\pi}{M_2}$. $E_{k_1k_2}$ and $\tilde{E}_{k_1k_2}$ can be calculated by 2D FFT:

$$E_{k_1k_2}^{pq}=\sum_{n_1=1}^{M_1}\sum_{n_2=1}^{M_2}D_{n_1n_2}^{pq}\,exp\left(i\frac{2\pi n_1k_1}{M_1}+i\frac{2\pi n_2k_2}{M_2}\right) \tag{26}$$

$$\tilde{E}_{k_1k_2}^{pq}=\sum_{n_1=1}^{M_1}\sum_{n_2=1}^{M_2}\tilde{D}_{n_1n_2}^{pq}\,exp\left(i\frac{2\pi n_1k_1}{M_1}-i\frac{2\pi n_2k_2}{M_2}\right) \tag{27}$$

in which

$$D_{n_1n_2}^{pq}=\begin{cases}2a_p(\kappa_{n_1},\omega_{n_2})b_q(\omega_{n_2})\sqrt{\Delta\kappa\Delta\omega}\,exp\left(i\phi_{n_1n_2}^{(1)}\right) & 1\leq n_1\leq M_1, 1\leq n_2\leq M_2\\ 0 & \text{others}\end{cases} \tag{28}$$

$$\tilde{D}_{n_1n_2}^{pq}=\begin{cases}2a_p(\kappa_{n_1},\omega_{n_2})b_q(\omega_{n_2})\sqrt{\Delta\kappa\Delta\omega}\,exp\left(i\phi_{n_1n_2}^{(2)}\right) & 1\leq n_1\leq M_1, 1\leq n_2\leq M_2\\ 0 & \text{others}\end{cases} \tag{29}$$

From above equations, space and time variables can be separated from frequency and wavenumber variables via POD decomposition on the wavenumber-frequency spectrum. $N_p\cdot N_q$ times 2D FFT need to be conducted on one sample simulation. Since the truncation order is low, often the first several modes contain most of the energy, only several 2D FFT is requested. So, the arithmetic speed of proposed method is obviously faster than the direct summation of trigonometric series. The flow chart of the proposed algorithm is shown in Fig. 1.

3. Application to wind velocity field along a 1-D transmission line

To validate the proposed method, a numerical simulation of a one-spatial dimensional nonstationary longitudinal wind field with time-varying coherence on transmission tower-line model is carried out. As shown in Fig.2, the height difference of each point in transmission line is ignored. The span of transmission line is 1000m, and 1000 simulating points at equal intervals of 1m on the transmission line are simulated by the proposed method. Consider the time-varying characteristics of the coherence function between each point, and the time-varying coherence function is shown by Eq. (4).

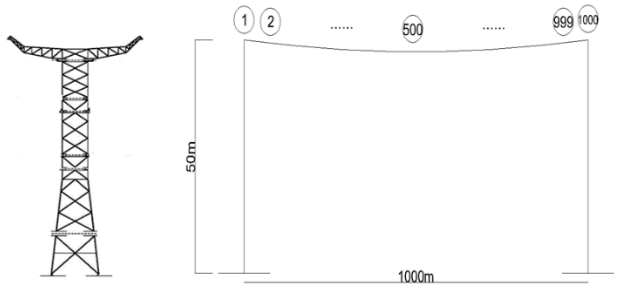

Fig. 2 Transmission tower-line model

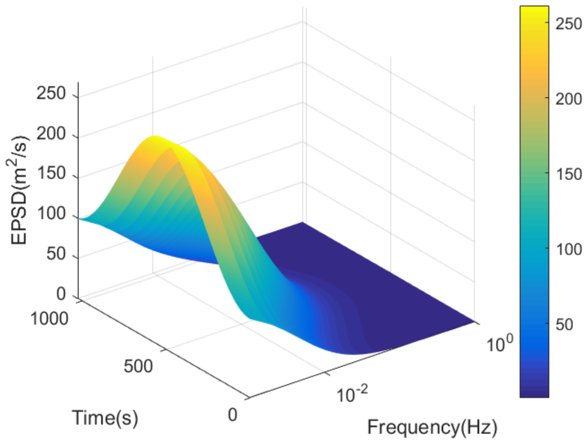

Fig. 3 The evolutionary power spectral density

Evolutionary power spectrum and the time-varying coherence function can be obtained by updating the time-varying mean winds (Kitagawa *et al.* 2003). Take Kaimal power spectrum as an example (Peng *et al.* 2017):

$$S(\omega,t)=\frac{200u_*(t)^2z}{2\pi\bar{U}(t)\left[1+50\dfrac{z\omega}{2\pi\bar{U}(t)}\right]^{5/3}} \tag{30}$$

where $u_*=\frac{K\bar{U}(t)}{ln(z/z_0)}$, $\bar{U}(t)$ is the time-varying mean wind velocity which satisfies $\bar{U}(t)=U_0\cdot d(t)$, $d(t)=1+\alpha\cos(\omega' t)$ with α=0.4, ω'=0.006. At the height z=50m, the designing wind velocity $U_0=30\text{m/s}$, Karman constant K=0.4. To simulate the non-uniformity of power spectral density, in general, the surface roughness for the length between points 1 to 500 is assumed $z_0=0.001$, while $z_0=0.005$ is assumed for the length between points 501 to 1000. The upper limit of cut-off frequency is $\omega_{up}=2\pi$ with discrete points in frequency domain N_ω=1024, the upper limit of cut-off wavenumber is $\kappa_{up}=\pi$, with discrete points in wavenumber domain N_κ=1024, the time interval is Δt=0.5s and the interval distance among simulating points is Δx=1m.

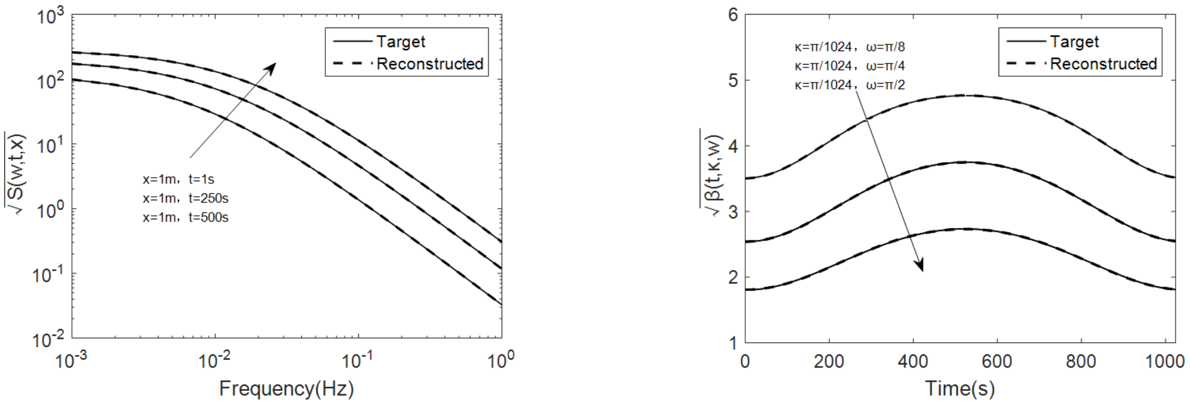

Fig. 4 The comparison between the reconstructed and target spectra

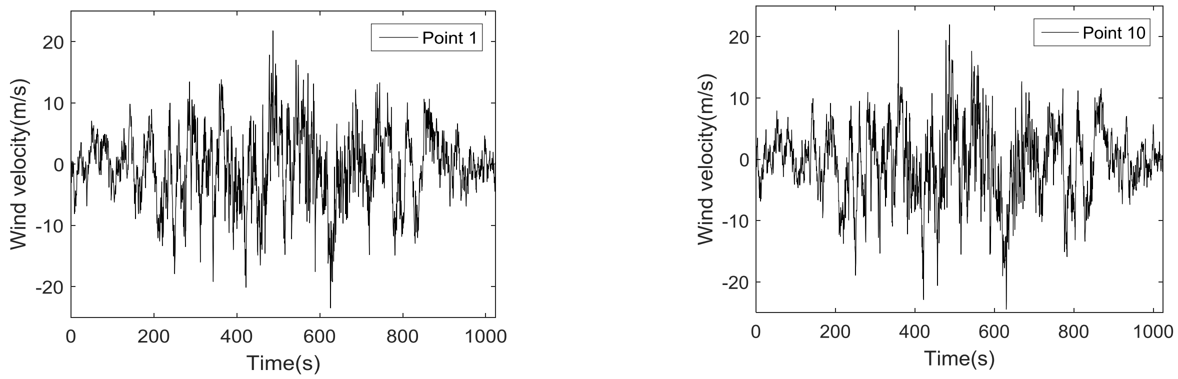

(a) The time history of fluctuating wind velocity at the 1st point

(b) The time history of fluctuating wind velocity at the 10th point

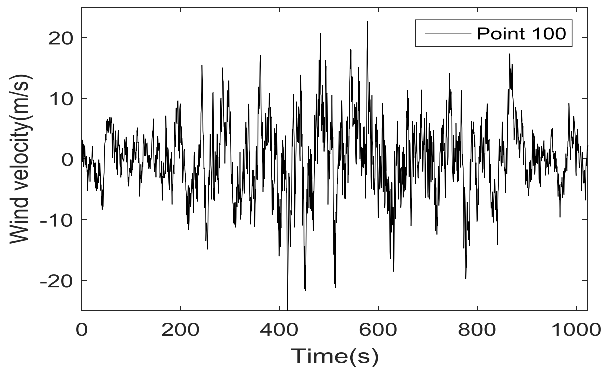

(c) The simulated time history of fluctuating wind velocity at the 100th point

Fig. 5 The time history of fluctuating wind velocity at different simulating points

It is worth noting that there are 1024 discrete points in wavenumber domain in this example, the number of simulation points in space domain is twice of discrete points in wavenumber domain, namely there are 2048 simulation points. Only the first 1000 simulation points are selected in this example. The selection of large discrete points in wavenumber domain is for the accurate simulation of wind field (Peng *et al.* 2017). Fig. 3 shows the evolutionary power spectral density with first 500 simulating points. It is clear that spectral density first increases with time and then decreases, the time-varying characteristic is obvious, and the energy is concentrated at high frequencies.

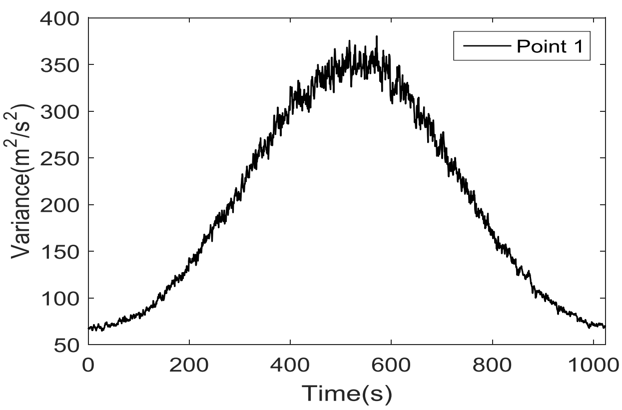

Fig. 6 The time-varying variance of the 1st point

Based on the proposed method, 1000 points of transmission line model in Fig.2 are simulated. Objective

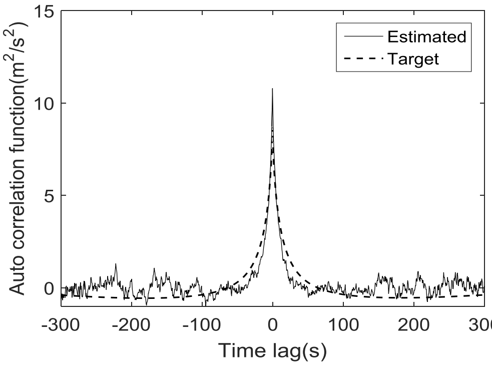

(a) Self-correlation of the 1st point

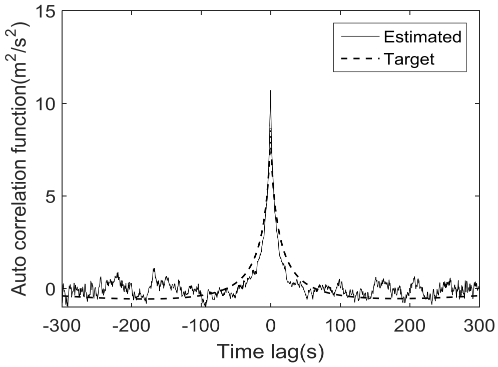

(b) Self-correlation of the 10th point

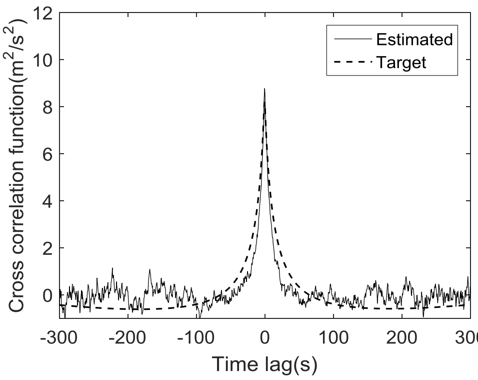

(c) Cross-correlation of the 1st and 10th points

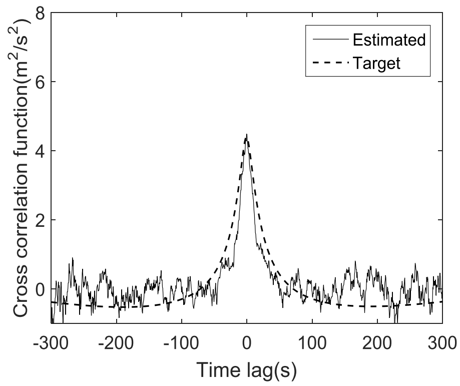

(d) Cross-correlation of the 1st and 100th points

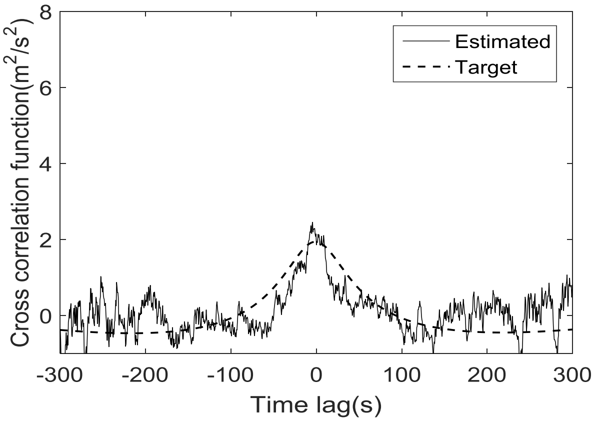

(e) Cross-correlation function of the 1st and 501th points

Fig. 7 The comparison of the self and cross-correlation functions at different points (t=100s)

function is carried out by POD decomposition using Eqs. (19-20). The first three eigenvalues of **P** and **Q** are 4.41, 0.014, 3.4×10^{-5} and 306.31, 3.05, 0.019 respectively. It is obvious that the first three modes contain the most energy of objective matrix. The comparison between the reconstructed values and the target values using the first three modes are shown in Fig.4, and it is demonstrated that the objective function can be reconstructed accurately by the first three modes.

The simulated time history of fluctuating wind velocity at the 1st, 10th and 100th points are shown in Fig.5. The nonstationary characteristic of wind velocity is obvious. The variance of the 1st point at different times is shown in Fig.6, which first increases and then decreases with time, and reaches the maximums at 512s.

The self-correlation function and cross-correlation function of two simulating points are calculated by:

$$R_{ij}\left(t,t+\tau\right)=\mathrm{E}\left(u_i\left(t\right)\cdot u_j\left(t+\tau\right)\right) \tag{31}$$

in which $\mathrm{E}(\cdot)$ denotes expectation.

The correlation function is the joint function of time and time lag. The comparison of simulated self-correlation function, cross-correlation function and those of the target correlation function of the non-stationary wind field are shown in Fig.7. From Fig.7, the self-correlation function and cross-correlation function are obviously symmetrical and reach the maximums when time lag is zero. With the increasing of the distance between the simulating points, the peak value of the cross-correlation function decreases

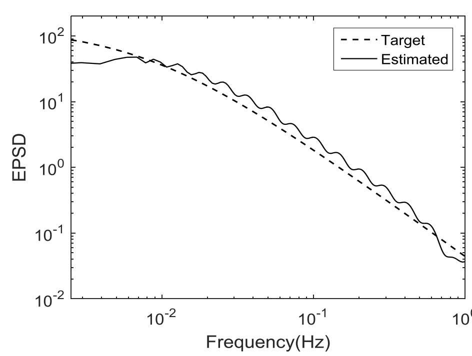

(a) EPSD of the 1st point (t=100s)

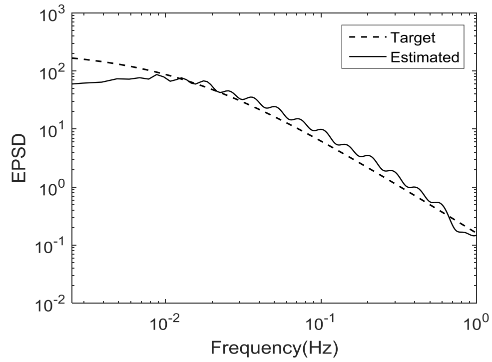

(b) EPSD of the 1st point (t=400s)

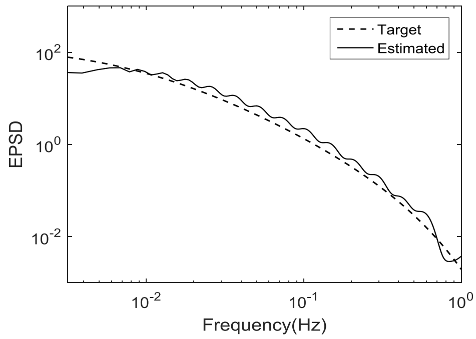

(c) EPSD between the 1st and 10th point (t=100s)

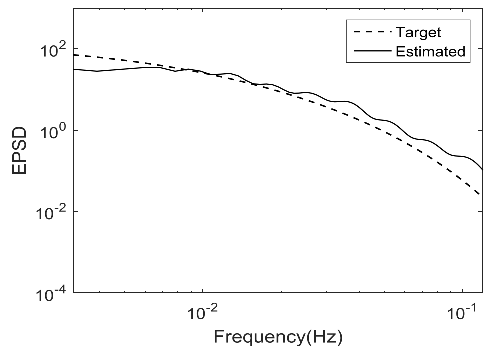

(d) EPSD between the 1st and 100th point (t=100s)

Fig. 8 The comparison of the EPSD and target value of different points

gradually, which conforms to the feature that correlation decreases with the increase of distance. The wavelets-based approach for estimating EPSD functions of nonstationary processes is adopted (Huang and Chen, 2009) and the comparison with target value are displayed in Fig.8. From the comparisons, the correlation function and EPSD of the simulated nonstationary fluctuating wind by the proposed method is well matched with the target values, which validate the effectiveness and accuracy of the proposed method.

4. Conclusions

Generally, the coherence function of the multivariate nonstationary process is time-varying, but current limited studies on the simulation of nonstationary fluctuating wind field with time-varying coherence are based on the traditional spectral representation method, which is inefficient for the simulation of multi-variable wind field to large span structures such as transmission tower-line. In this paper, an efficient method is proposed for the numerical simulation of nonstationary fluctuating wind field in one-spatial dimension with time-varying coherence via the hybrid wavenumber-frequency spectrum and proper orthogonal decomposition. Based on the transformation relation between evolutionary power spectrum density and wavenumber-frequency spectrum for nonstationary process with time-varying coherence function, the simulation by wave number frequency spectrum is derived. The Cholesky decomposition in the traditional spectral representation method which may lead to the singular error is completely avoided. Moreover, the efficient proper orthogonal decomposition decomposes the time-dependent and space-dependent evolutionary power spectrum density and the Fourier transform of time-varying coherent function simultaneously, so that the two-dimensional Fast Fourier transform can be applied in trigonometric series superposition to further enhance simulation efficiency greatly. This proposed algorithm is preferable for wind field simulation of long-span structures with large simulation numbers. A numerical example of simulating the multi-variable nonstationary wind field with time-varying coherence along the longitudinal transmission tower line model has validated that the proposed method can simulate the nonstationary wind field efficiently and accurately, which provides a basis for the dynamic response analysis of the transmission tower-line system under nonstationary wind excitations.

Acknowledgments

This research is financially supported by the National Key R&D Program of China through the Grant No. 2017YFC0803300.

References

Bao, X. and Li, C.X. (2019), "Fast simulation of non-stationary wind velocity based on time-frequency interpolation", *J. Wind Eng. Ind. Aerodyn.*, **193**, 103982.

https://doi.org/10.1016/j.jweia.2019.103982.

Bao, X. and Li, C.X. (2020), "Application of Time-Frequency Interpolation and Proper Orthogonal Decomposition in Nonstationary Wind-Field Simulation". *J. Eng. Mech.,* **146**(5), 04020034. https://doi.org/10.1061/(ASCE)EM.1943-7889.0001761.

Benowitz, B.A.and Deodatis, G. (2015), "Simulation of wind velocities on long span structures: a novel stochastic wave based model", *J. Wind Eng. Ind. Aerod.* **147**, 154–163. https://doi.org/10.1016/j.jweia.2015.10.004.

Chen, J.B., Song, Y. P., Peng, Y.B. and Spanos, P.D. (2018), "Simulation of Homogeneous Fluctuating Wind Field in Two Spatial Dimensions via a Joint Wave Number-Frequency Power Spectrum", *J. Eng. Mech*, **144**(11),04018100. https://doi.org/10.1061/(ASCE)EM.1943-7889.0001525.

Deodatis, G. and Shinozuka, M. (1989), "Simulation of Seismic Ground Motion Using Stochastic Waves", *J. Eng. Mech*, **115**(12), 2723-2737. https://doi.org/10.1061/(ASCE)0733-9399(1989)115:12(2723).

Ding, Q.S., Zhu, L.D. and Xiang, H.F. (2006), "Simulation of stationary Gaussian stochastic wind velocity field", *Wind Struct.*, **9**(3), 231-243. https://doi.org/10.12989/was.2006.9.3.231.

Huang, Z.F., Xu, Y.L., Tao, T.Y. and Zhan, S. (2020), "Time-varying power spectra and coherences of non-stationary typhoon winds", *J. Wind Eng. Ind. Aerodyn*, **198**, 104115. https://doi.org/10.1016/j.jweia.2020.104115.

Huang, G.Q., Peng, L.L., Ahsan, Kareem. and Song, C.C. (2020), "Data-driven simulation of multivariate nonstationary winds: A hybridmultivariate empirical mode decomposition and spectral representation method", *J. Wind Eng. Ind. Aerodyn*, **197**,104073. https://doi.org/10.1016/j.jweia.2019.104073.

Huang, G.Q. and Chen, X.Z. (2009), "Wavelets-based estimation of multivariate evolutionary spectra and its application to nonstationary downburst winds", *Eng. Struct,*, **31**(4), 976-989. https://doi.org/10.1016/j.engstruct.2008.12.010.

Huang, G.Q. (2014), "An efficient simulation approach for multivariate nonstationary process: Hybrid of wavelet and spectral representation method", *Probab. Eng. Mech*, **34**,74-83. https://doi.org/10.1016/j.probengmech.2014.06.001.

Huang, G.Q., Zheng, H., Xu, Y.L. and Li Y.L. (2015), "Spectrum models for nonstationary extreme winds", *J. Struct. Eng*, **141**(10), 04015010. https://doi.org/10.1061/(ASCE)ST.1943-541X.0001257.

Kitagawa, T. and Nomura, T. (2003), "A wavelet-based method to generate artificial wind fluctuation data", *J. Wind Eng. Ind. Aerodyn*, **91**(7), 943-964. https://doi.org/10.1016/S0167-6105(03)00037-0.

Li, J., Peng, Y.B. and Yan, Q. (2013), "Modeling and simulation of fluctuating wind speeds using evolutionary phasespectrum", *Probab. Eng. Mech*, **32**, 48-55. https://doi.org/10.1016/j.probengmech.2013.01.001.

Li, Y.L., Togbenou, K., Xiang, H.Y. and Chen, N. (2017), "Simulation of non-stationary wind velocity field on bridges based on Taylor series", *J. Wind Eng. Ind. Aerodyn*, **169**, 117-127. https://doi.org/10.1016/j.jweia.2017.07.005.

Liang, J.W., Chaudhuri, S.R., and Shinozuka, M (2007), "Simulation of nonstationary stochastic processes by spectral representation", *J. Eng. Mech*, **133**(6),616-627. https://doi.org/10.1061/(ASCE)0733-9399(2007)133:6(616).

Lin, L., Ang, AHS., Xia, D.D., Hu, H.T., Wang, H.F, and He, F.Q. (2017), "Fluctuating wind field analysis based on random Fourier spectrum for wind induced response of high-rise structures", *Struct. Eng. Mech.,* **63**(6) 837-846. https://doi.org/10.12989/sem.2017.63.6.837.

Lin, L., Chen, K., Xia, D.D., Wang, H.F., Hu, H.T. and He, F.Q. (2018), "Analysis on the wind characteristics under typhoon climate at the southeast coast of China", *J. Wind Eng. Ind. Aerodyn*, **182**, 37-48. https://doi.org/10.1016/j.jweia.2018.09.003.

Liu, Z.J., Liu, W. and Peng, Y. B. (2016), "Random function based spectral representation of stationary and non-stationary stochastic processes", *Probab. Eng. Mech*., **45**, 115–126. https://doi.org/10.1016/j.probengmech.2016.04.004.

Peng, L.L., Huang, G.Q., Chen, X.Z. and Kareem, A. (2017), "Simulation of multivariate nonstationary random processes: hybrid stochastic wave and proper orthogonal decomposition approach", *J. Eng. Mech*, **143**(9),04017064. https://doi.org/10.1061/(ASCE)EM.1943-7889.0001273.

Peng, L.L., Huang, G.Q., Chen, X.Z. and Yang, Q.S. (2018), "Evolutionary Spectra-Based Time-Varying Coherence Function and Application in Structural Response Analysis to Downburst Winds", *J. Struct. Eng*, **14**4(7),04018078. https://doi.org/10.1061/(ASCE)ST.1943-541X.0002066.

Priestley, M.B. (1965),"Evolutionary spectra and non-stationary processes", *J. Royal Statistical Soc. Series B (Methodological)* , **27**, 204-237. https://doi.org/10.1111/j.2517-6161.1965.tb01488.x.

Song, Y.P., Chen, J.B., Peng,Y.B., Spanos, P. D. and Li, J. (2018), "Simulation of nonhomogeneous fluctuating wind speed field in two-spatial dimensions via an evolutionary wavenumber-frequency joint power spectrum", *J. Wind Eng. Ind. Aerodyn*, **179**, 250-259. https://doi.org/10.1016/j.jweia.2018.06.005.

Song, Y.P., Chen, J.B. and Peng, Y.B. (2019),"Simulation of nonhomogeneous fluctuating wind field in one-dimensional space by evolutionary wavenumber-frequency joint power spectrum", *J. Eng.Mech*, **36**(2), 208-217. https://doi.org/10.22725/ICASP13.126.

Tao, T.Y., Wang, H., Yao, C., He, X. and Kareem, A. (2018), "Efficacy of Interpolation-Enhanced Schemes in Random Wind Field Simulation over Long-Span Bridges", *J. Bridge Eng.*, **23**(3), 04017147. https://doi.org/10.1061/(ASCE)BE.1943-5592.0001203.

Tao, T.Y., Wang, H. and Kareem, A. (2018), "Reduced-Hermite bifold-interpolation assisted schemes for the simulation of random wind field", *Probab. Eng. Mech*, **53**, 126-142. https://doi.org/10.1016/j.probengmech.2018.08.002.

Tao, T.Y. and Wang, H. (2019), "Modelling of longitudinal evolutionary power spectral density of typhoon winds considering high-frequency subrange", *J. Wind Eng. Ind. Aerodyn*, **193**, 103957. https://doi.org/10.1016/j.jweia.2019.103957.

Wu, Y.X., Gao, Y.F., Zhang, N. and Zhang, F. (2018), "Simulation of spatially varying non-Gaussian and non-stationary seismic ground motions by the spectral representation method", *J. Eng. Mech.,* **144**(1), 04017143. https://doi.org/10.1061/(ASCE)EM.1943-7889.0001371.

Wu, Y. and Gao, Y. (2019),"A modified spectral representation method to simulate non-Gaussian random vector process considering wave-passage effect", *Eng. Struct*, **201**, 109587. https://doi.org/10.1016/j.engstruct.2019.109587.

Zentner, I., Ferré, G., Poirion, F. and Benoit, M. (2016), "A biorthogonal decomposition for the identification and simulation of non-stationary and non-Gaussian random fields", *J. Comput. Phys*, **314**, 1-13. https://doi.org/10.1016/j.jcp.2016.02.067.

Zhao, N. and Huang, G.Q. (2017), "Fast simulation of multivariate nonstationary process and its application to extreme winds", *J. Wind Eng. Ind. Aerodyn.*, **170**, 118-127. https://doi.org/10.1016/j.jweia.2017.08.008.

CC